1

Introduction

1.1 Materials Processing

Chemically reactive plasma discharges are widely used to modify the surface properties of materials. Plasma processing technology is vitally important to several of the largest manufacturing industries in the world. Plasma-based surface processes are indispensable for manufacturing the very large-scale integrated circuits (ICs) used by the electronics industry. Such processes are also critical for the flat panel display, solar panel, aerospace, automotive, steel, biomedical, and toxic waste management industries. Materials and surface structures can be fabricated that are not attainable by any other commercial method, and the surface properties of materials can be modified in unique ways. For example, 0.2-μm-wide, 4-μm-deep trenches can be etched into silicon films or substrates (Figure 1.1*a*). A human hair is 50–100 μm in diameter, so hundreds of these trenches would fit endwise within a human hair. A more recent example in Figure 1.1*b* shows a set of approximately 0.1 μm in diameter by 7.5 μm deep channel holes etched into a stacked set of dielectric layers. Unique materials such as diamond films and amorphous silicon for solar cells have also been produced, and plasma-based hardening of surgically implanted hip joints and machine tools have extended their working lifetimes manyfold.

It is instructive to look closer at IC fabrication, which is the key application driving the field that we describe in this book. As a very incomplete list of plasma processes, argon or oxygen discharges are used to sputter-deposit aluminum, tungsten, or high-temperature superconducting films; oxygen discharges can be used to grow SiO_2 films on silicon; SiH_2Cl_2/NH_3 and $Si(OC_2H_5)_4/O_2$ discharges are used for the plasma-enhanced chemical vapor deposition (PECVD) of Si_3N_4 and SiO_2 films, respectively; BF_3 discharges can be used to implant dopant (B) atoms into silicon; $CF_4/Cl_2/O_2$ discharges are used to selectively remove silicon films; and oxygen discharges are used to remove photoresist or polymer films. These types of steps (deposit or grow, dope or modify, etch or remove) are repeated again and again in the manufacture of a modern IC. They are the equivalent, on a submicrometer-size scale, of centimeter-size manufacture using metal and components, bolts and solder, and drill press and lathe. For microfabrication of an IC, one-third of the tens to hundreds of fabrication steps are typically plasma-based.

Figure 1.2 shows a typical set of steps to create a metal film patterned with submicrometer features on a large-area (300 mm diameter) wafer substrate. In (*a*), the film is deposited; in (*b*), a photoresist layer is deposited over the film; in (*c*), the resist is selectively exposed to light through a pattern; and in (*d*), the resist is developed, removing the exposed resist regions and leaving behind

Principles of Plasma Discharges and Materials Processing, Third Edition. Michael A. Lieberman and Allan J. Lichtenberg.

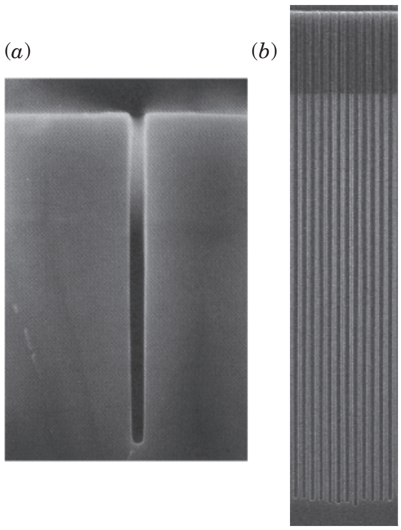

Figure 1.1 High aspect ratio anisotropic etches, showing the extraordinary capabilities of plasma processing; such etched features are used for device isolation, charge storage capacitors, channel holes, and many other purposes in integrated circuits: (*a*) trench etch (0.2 μm wide by 4 μm deep) in single-crystal silicon, circa 2004; (*b*) set of channel holes (each approximately 0.1 μm in diameter by 7.5 μm deep) etched into a stacked set of dielectric layers, circa 2023. Source: (*a*) M. A. Lieberman (Book Author). (*b*) Courtesy of Lam Research Corporation.

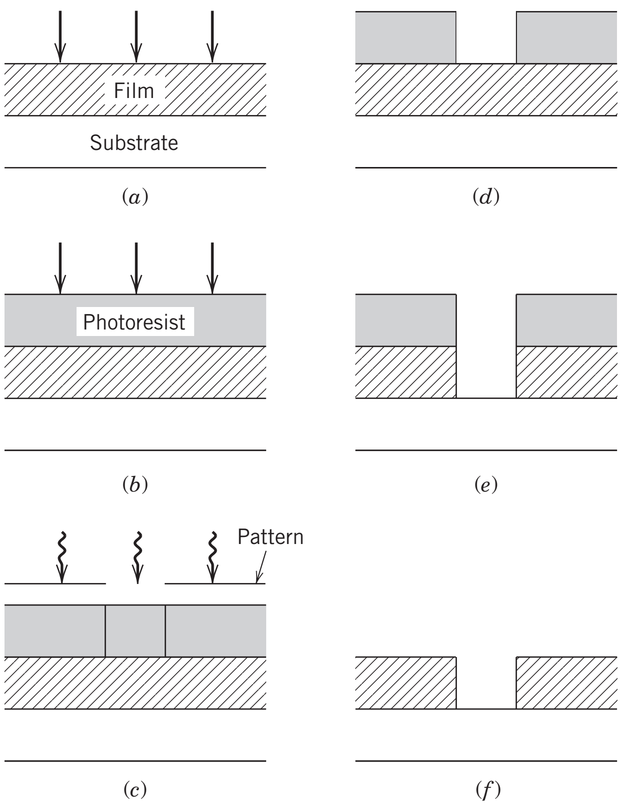

Figure 1.2 Deposition and pattern transfer in manufacturing an integrated circuit: (*a*) metal deposition; (*b*) photoresist deposition; (*c*) optical exposure through a pattern; (*d*) photoresist development; (*e*) anisotropic plasma etch; (*f*) remaining photoresist removal.

a patterned resist mask. In (*e*), this pattern is transferred into the film by an etch process; the mask protects the underlying film from being etched. In (*f*), the remaining resist mask is removed. Of these six steps, plasma processing is generally used for film deposition (*a*) and etch (*e*) and may also be used for resist development (*d*) and removal (*f*).

The etch process in (*e*) is illustrated as leading to vertical sidewalls aligned with the resist mask; i.e., the mask pattern has been faithfully transferred into the metal film. This can be accomplished by an etch process that removes material in the vertical direction only. The horizontal etch rate is zero. Such *anisotropic* etches are easily produced by plasma processing. On the other hand, one might imagine that exposing the masked film (*d*) to a liquid (or vapor phase) etchant will lead to the undercut *isotropic* profile shown in Figure 1.3*a* (compare to Figure 1.2*e*), which is produced by equal vertical and horizontal etch rates. Many years ago, feature spacings (e.g., between trenches) were tens of micrometers, much exceeding the required film thicknesses. Undercutting was then acceptable. This is no longer true with submicrometer feature spacings. The reduction in feature sizes and spacings makes anisotropic etch processes essential. In fact, strictly vertical etches are sometimes not desired; one wants controlled sidewall angles. Plasma processing is the only commercial technology capable of such control. Anisotropy is a critical process parameter in IC manufacture and has been a major force in driving the development of plasma processing technology.

The etch process applied to remove the film in Figure 1.2*d* is shown in Figure 1.2*e* as not removing either the photoresist or the underlying substrate. This selectivity is another critical process parameter for IC manufacture. Whereas wet etches have been developed having essentially infinite selectivity, highly selective plasma etch processes are not easily designed. Selectivity and anisotropy often compete in the design of a plasma etch process, with results as shown in Figure 1.3*b*. Compare this to the idealized result shown in Figure 1.2*e*. Assuming that film-to-substrate selectivity

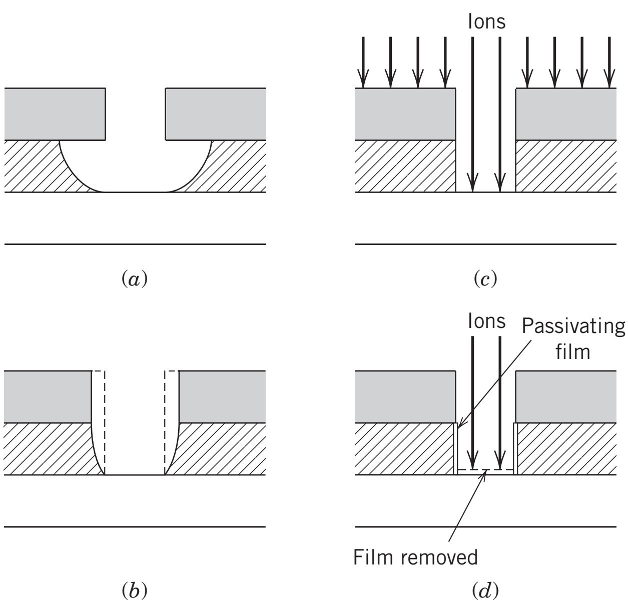

Figure 1.3 Plasma etching in integrated circuit manufacture: (*a*) example of isotropic etch; (*b*) sidewall etching of the resist mask leads to a loss of anisotropy in film etch; (*c*) illustrating the role of bombarding ions in anisotropic etch; (*d*) illustrating the role of sidewall passivating films in anisotropic etch.

is a critical issue, one might imagine simply turning off the plasma after the film has been etched through. This requires a good endpoint detection system. Even then, variations in film thickness and etch rate across the area of the wafer imply that the etch cannot be stopped at the right moment everywhere. Hence, depending on the process uniformity, there is a need for some selectivity. These issues are considered further in Chapter 16.

Here is a simple recipe for etching silicon using a plasma discharge. Start with an inert molecular gas, such as CF_4. Excite the discharge to sustain a plasma by electron–neutral dissociative ionization,

$$e + CF_4 \rightarrow 2e + CF_3^+ + F$$

and to create reactive species by electron–neutral dissociation,

$$\begin{aligned} e + CF_4 &\rightarrow e + F + CF_3 \\ &\rightarrow e + 2F + CF_2 \end{aligned}$$

The etchant F atoms react with the silicon substrate, yielding the volatile etch product SiF_4:

$$Si(s) + 4F(g) \rightarrow SiF_4(g)$$

Here, s and g indicate solid and gaseous forms, respectively. Finally, the product is pumped away. It is important that CF_4 does not react with silicon and that the etch product SiF_4 is volatile, so that it can be removed. This process etches silicon isotropically. For an anisotropic etch, there must be high-energy ion (CF_3^+) bombardment of the substrate. As illustrated in Figure 1.3*c* and *d*, energetic ions leaving the discharge during the etch bombard the bottom of the trench but do not bombard the sidewalls, leading to anisotropic etching by one of the two mechanisms. Either the ion bombardment increases the reaction rate at the surface (Figure 1.3*c*) or it exposes the surface to the etchant by removing passivating films that cover the surface (Figure 1.3*d*).

Similarly, Cl and Br atoms created by dissociation in a discharge are good etchants for silicon, F atoms and CF_2 molecules for SiO_2, O atoms for photoresist, and Cl atoms for aluminum. In all cases, a volatile etch product is formed. However, F atoms do not etch aluminum, and there is no commercially viable etchant for copper, because the etch products are not volatile at reasonable substrate temperatures.

We see the importance of the basic physics and chemistry topics treated in this book: (1) plasma physics (Chapters 2, 4–6, and 19) to determine the electron and ion densities, temperatures, and ion bombardment energies and fluxes for a given discharge configuration; and (2) gas-phase chemistry and (3) surface physics and chemistry (Chapters 7 and 9) to determine the etchant densities and fluxes and the etch rates with and without ion bombardment. The database for these fields of science is provided by (4) atomic and molecular physics, which we discuss in Chapters 3 and 8. We also discuss applications of equilibrium thermodynamics (Chapter 7) to plasma processing. The measurement and experimental control of plasma and chemical properties in reactive discharges is itself a vast subject. We provide brief introductions to some simple plasma diagnostic techniques throughout the text.

We have motivated the study of the fundamentals of plasma processing by examining isotropic and anisotropic etches for IC manufacture. These are discussed in Chapter 16. Other characteristics motivate its use for deposition and surface modification. For example, a central feature of the *low-pressure* processing discharges that we consider in this book is that the plasma itself, as well as the plasma–substrate system, is not in thermal equilibrium. This enables substrate temperatures to be relatively low, compared to those required in conventional thermal processes, while maintaining adequate deposition or etch rates. Putting it another way, plasma processing rates are greatly

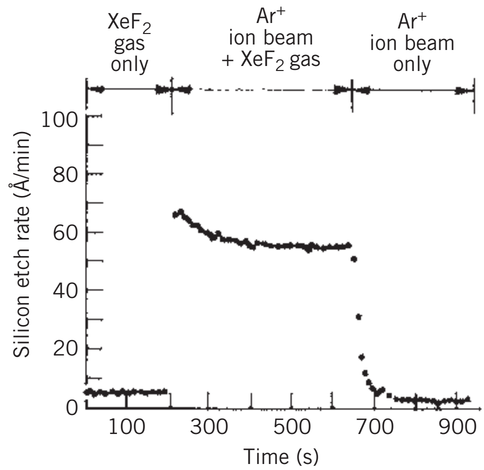

Figure 1.4 Experimental demonstration of ion-enhanced plasma etching. Source: Adapted from Coburn and Winters (1979).

enhanced over thermal processing rates at the same substrate temperature. For example, Si_3N_4 films can be deposited over aluminum films by PECVD, whereas adequate deposition rates cannot be achieved by conventional chemical vapor deposition (CVD) without melting the aluminum film. Chapter 17 gives further details.

Particulates or "dust" can be a significant component in processing discharges and a source of substrate-level contamination in etch and deposition processes. One can also control dust formation in useful ways, for example, to produce powders of various sizes or to incorporate nanoparticles during deposition to modify film properties. Dusty plasmas are described in Chapter 18.

The nonequilibrium nature of plasma processing has been known for many years, as illustrated by the laboratory data in Figure 1.4. In time sequence, this shows first, the equilibrium chemical etch rate of silicon in the XeF_2 etchant gas; next, the tenfold increase in etch rate with the addition of argon ion bombardment of the substrate, simulating plasma-assisted etching; and finally, the very low "etch rate" due to the physical sputtering of silicon by the ion bombardment alone.

Another application is the use of plasma-immersion ion implantation (PIII) to implant ions into materials at dose rates that are tens to hundreds of times larger than those achievable with conventional (beam-based) ion implantation systems. In PIII, a series of negative high-voltage pulses are applied to a substrate that is immersed directly into a discharge, thus accelerating plasma ions into the substrate. The development of PIII has opened a new implantation regime characterized by very high dose rates, even at very low energies, and by the capability to implant both large-area and irregularly shaped substrates, such as flat panel displays or machine tools and dies. This is illustrated in Figure 1.5. Further details are given in Chapter 17.

1.2 Plasmas and Sheaths

1.2.1 Plasmas

A plasma is a collection of free charged particles moving in random directions, that is, on an average, electrically neutral (see Figure 1.6*a*). This book deals with weakly ionized plasma discharges, which are plasmas having the following features: (1) they are driven electrically; (2) charged particle collisions with neutral gas molecules are important; (3) there are boundaries at which surface

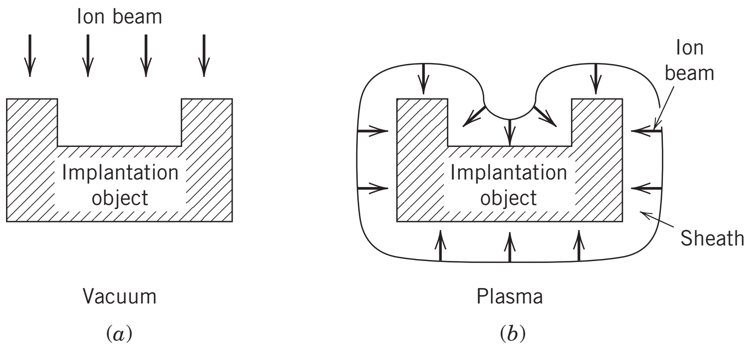

Figure 1.5 Illustrating ion implantation of an irregular object: (*a*) in a conventional ion beam implanter, the beam is electrically scanned and the target object is mechanically rotated and tilted to achieve uniform implantation; (*b*) in plasma-immersion ion implantation (PIII), the target is immersed in a plasma, and ions from the plasma are implanted with a relatively uniform spatial distribution.

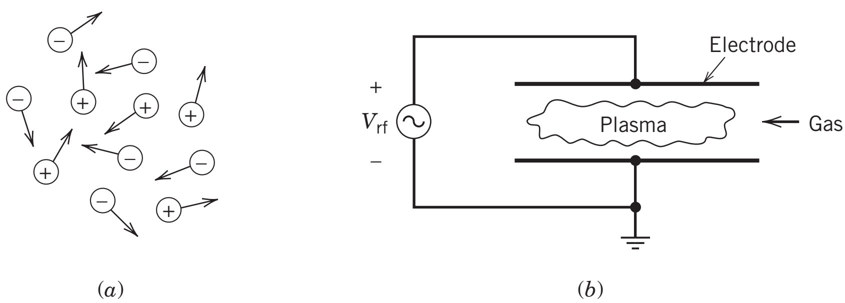

Figure 1.6 Schematic view of (*a*) a plasma and (*b*) a discharge.

losses are important; (4) ionization of neutrals sustains the plasma in the steady state; and (5) the electrons are not in thermal equilibrium with the ions.

A simple discharge is shown schematically in Figure 1.6*b*. It consists of a voltage source that drives current through a low-pressure gas between two parallel conducting plates or electrodes. The gas "breaks down" to form a plasma, usually weakly ionized, i.e., the plasma density is only a small fraction of the neutral gas density. We describe some qualitative features of plasmas in this section; discharges are described in the following section.

Plasmas are often called a fourth state of matter. As we know, a solid substance in thermal equilibrium generally passes into a liquid state as the temperature is increased at a fixed pressure. The liquid passes into a gas as the temperature is further increased. At a sufficiently high temperature, the molecules in the gas decompose to form a gas of atoms that move freely in random directions, except for infrequent collisions between atoms. If the temperature is further increased, then the atoms decompose into freely moving charged particles (electrons and positive ions), and the substance enters the plasma state. This state is characterized by a common charged particle density $n_\mathrm{e} \approx n_\mathrm{i} \approx n$ particles/m^3 and, in equilibrium, a common temperature for all species. The temperatures required to form plasmas from pure substances in thermal equilibrium range from roughly 4000 K for easy-to-ionize elements like cesium to 20,000 K for hard-to-ionize elements like helium. The fractional ionization of a plasma is

$$x_\mathrm{iz} = \frac{n_\mathrm{i}}{n_\mathrm{g} + n_\mathrm{i}}$$

where n_g is the neutral gas density, x_{iz} is near unity for fully ionized plasmas, and $x_{iz} \ll 1$ for weakly ionized plasmas.

Much of the matter in the universe is in the plasma state. This is true because stars, as well as most interstellar matter, are plasmas. Although stars are plasmas in thermal equilibrium, the light and heavy charged particles in low-pressure processing discharges are *almost never* in thermal equilibrium, either between themselves or with their surroundings. Because these discharges are electrically driven and are weakly ionized, the applied power preferentially heats the mobile electrons, while the heavy ions efficiently exchange energy by collisions with the cold background gas. Hence, $T_e \gg T_i$ for these plasmas.

Figure 1.8 identifies different kinds of plasmas on a $\log_{10} n$ versus $\log_{10} T_e$ diagram. There is an enormous range of densities and temperatures for both laboratory and space plasmas. Two important types of processing discharges are indicated in the figure. Low-pressure glow discharges are characterized by $T_e \approx 1$–10 V, $T_i \ll T_e$, and $n \approx 10^8$–10^{13} cm^{-3}. These discharges are used as miniature chemical factories in which feedstock gases are broken into positive ions and chemically reactive etchants, deposition precursors, etc., which then flow to and physically or chemically react at the substrate surface. While energy is delivered to the substrate also, e.g., in the form of bombarding ions, the energy flux is there to promote the chemistry at the substrate and not to heat the substrate. The gas pressures for these discharges are low: $p \approx 1$ mTorr–1 Torr. *These discharges and their use for processing are the principal subject of this book.* We give the quantitative framework for their analysis in Chapter 10.

As shown in Figure 1.7, at low pressures, the electrons are *not* in thermal equilibrium with the ions. Because of the very light mass of electrons compared to ions and neutrals, $m/M \sim 10^{-4}$, the energy transfer during electron collisions with heavy particles is very weak. Since mainly electrons are heated by the applied fields, $T_e \gg T_i$ in the plasma. At the same time, ions can acquire high energies $\mathcal{E}_i$ by acceleration across sheaths near the substrate surface, $\mathcal{E}_i \gg T_e$. This enables "high temperature processing at low temperatures." The substrate can be kept near room temperature, with the hot electrons producing both chemically reactive species and energetic ions bombarding the substrate.

High-pressure arc discharges, shown in Figure 1.8, are also used for processing. These discharges have $T_e \approx 0.1$–2 V and $n \approx 10^{14}$–10^{19} cm^{-3}, and the light and heavy particles are more nearly in thermal equilibrium, with $T_i \lesssim T_e$. These discharges are used mainly to deliver heat to the substrate, e.g., to increase surface reaction rates, to melt, sinter, or evaporate materials, or to weld or cut refractory materials. Operating pressures are typically near atmospheric pressure (760 Torr). High-pressure discharges of this type are beyond the scope of this book.

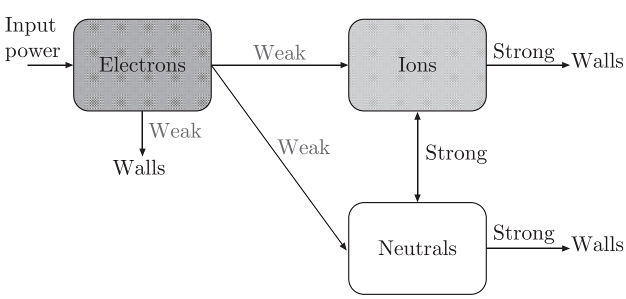

Figure 1.7 Energy coupling between electrons and heavy particles in a low-pressure plasma.

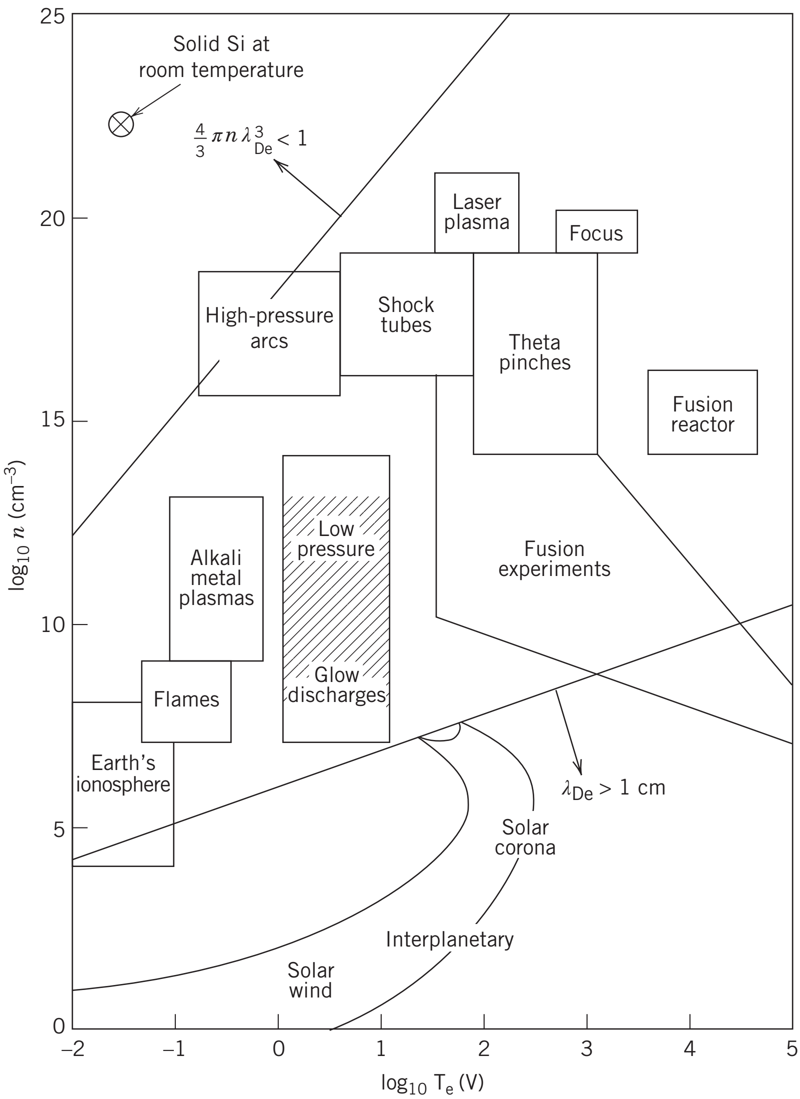

Figure 1.8 Space and laboratory plasmas on a $\log_{10} n$ versus $\log_{10} T_e$ diagram (Source: Book (1987)/Naval Research Laboratory); the electron Debye length λ_{De} is defined in Section 2.4.

Figure 1.9 shows the densities and temperatures (or average energies) for various species in a typical rf-driven, capacitively coupled low-pressure discharge, e.g., for silicon etching using CF_4, as described in Section 1.1. We see that the feedstock gas, etchant atoms, etch product gas, and plasma ions have roughly the same temperature, which does not exceed a few times room temperature (0.026 V). The etchant F and product SiF_4 densities are significant fractions of the CF_4 density, but the fractional ionization is very low: $n_i \sim 10^{-5} n_g$. The electron temperature T_e is two orders of magnitude larger than the ion temperature T_i. However, we note that the energy of ions bombarding the substrate can be 100–1000 V, much exceeding T_e. The acceleration of low-temperature ions across a thin *sheath* region where the plasma and substrate meet is central to all processing discharges. We describe this qualitatively next and quantitatively in later chapters.

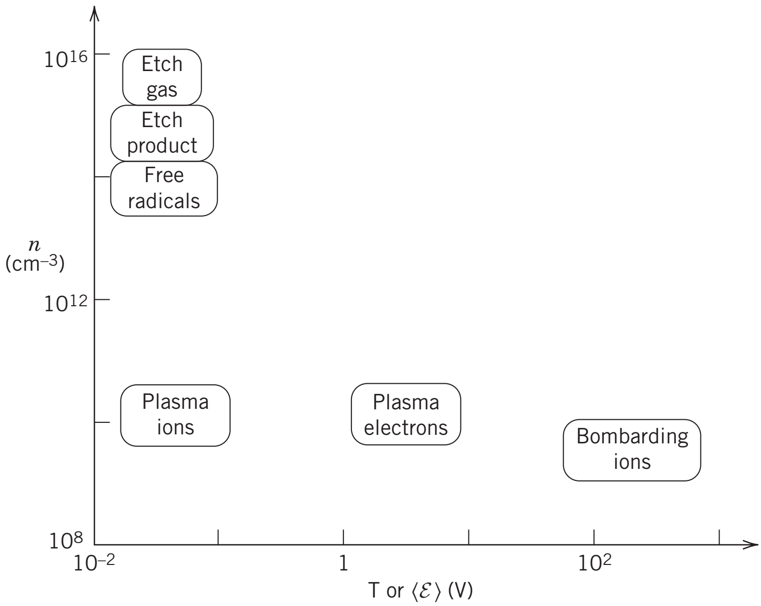

Figure 1.9 Densities and energies for various species in a low-pressure capacitive rf discharge.

Although n_i and n_e may be five orders of magnitude lower than n_g, the charged particles play central roles in sustaining the discharge and in processing. Because $T_e \gg T_i$, it is the electrons that dissociate the feedstock gas to create the free radicals, etchant atoms, and deposition precursors, required for the chemistry at the substrate. Electrons also ionize the gas to create the positive ions that subsequently bombard the substrate. As we have seen, energetic ion bombardment can increase chemical reaction rates at the surface, clear inhibitor films from the surface, and physically sputter materials from or implant ions into the surface.

T_e is generally less than the threshold energies $\mathcal{E}_{diss}$ or $\mathcal{E}_{iz}$ for dissociation and ionization of the feedstock gas molecules. Nevertheless, dissociation and ionization occur because electrons have a distribution of energies. Let $g_e(\mathcal{E})\, d\mathcal{E}$ be the number of electrons per unit volume with energies lying between $\mathcal{E}$ and $\mathcal{E} + d\mathcal{E}$, then the distribution function $g_e(\mathcal{E})$ is sketched in Figure 1.10. Electrons having energies below $\mathcal{E}_{diss}$ or $\mathcal{E}_{iz}$ cannot dissociate or ionize the gas. We see that dissociation and ionization are produced by the high-energy tail of the distribution. Although the distribution is sketched in the figure as if it were Maxwellian at the bulk electron temperature T_e, this may

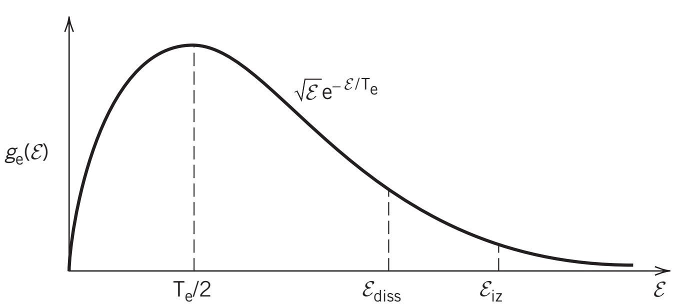

Figure 1.10 Electron energy distribution function $g_e(\mathcal{E})$ in a weakly ionized discharge.

not be the case. The tail distribution might be depressed below or enhanced above a Maxwellian by electron heating and electron–neutral collision processes. Two temperature distributions are sometimes observed, with T_e for the bulk electrons lower than T_h for the energetic electron tail. Non-Maxwellian distributions can only be described using the kinetic theory of discharges, which we introduce in Chapter 19.

1.2.2 Sheaths

Plasmas, which are quasineutral ($n_i \approx n_e$), are joined to wall surfaces across thin positively charged layers called *sheaths*. To see why, first note that the electron thermal velocity $(eT_e/m)^{1/2}$ is at least 100 times the ion thermal velocity $(eT_i/M)^{1/2}$ because $m/M \ll 1$ and $T_e \gtrsim T_i$. (Here, T_e and T_i are given in units of volts.) Consider a plasma of width l with $n_e = n_i$ initially confined between two grounded ($\Phi = 0$) absorbing walls (Figure 1.11*a*). Because the net charge density $\rho = e(n_i - n_e)$ is zero, the electric potential Φ and the electric field E_x are zero everywhere. Hence, the fast-moving electrons are not confined and will rapidly be lost to the walls. On a very short timescale, however, some electrons near the walls are lost, leading to the situation shown in Figure 1.11*b*. Thin ($s \ll l$) positive ion sheaths form near each wall in which $n_i \gg n_e$. The net positive ρ within the sheaths leads to a potential profile $\Phi(x)$ that is positive within the plasma and falls sharply to zero near both walls. This acts as a confining potential "valley" for electrons and a "hill" for ions because the electric fields within the sheaths point from the plasma to the wall. Thus, the force $-eE_x$ acting on electrons is directed into the plasma; this reflects electrons traveling toward the walls back into the plasma. Conversely, ions from the plasma that enter the sheaths are accelerated into the walls. If the plasma potential (with respect to the walls) is V_p, then we expect that $V_p \sim$ a few T_e in order to confine most of the electrons. The energy of ions bombarding the walls is then $\mathcal{E}_i \sim$ a few T_e. Charge uncovering is treated quantitatively in Chapter 2 and sheaths in Chapter 6.

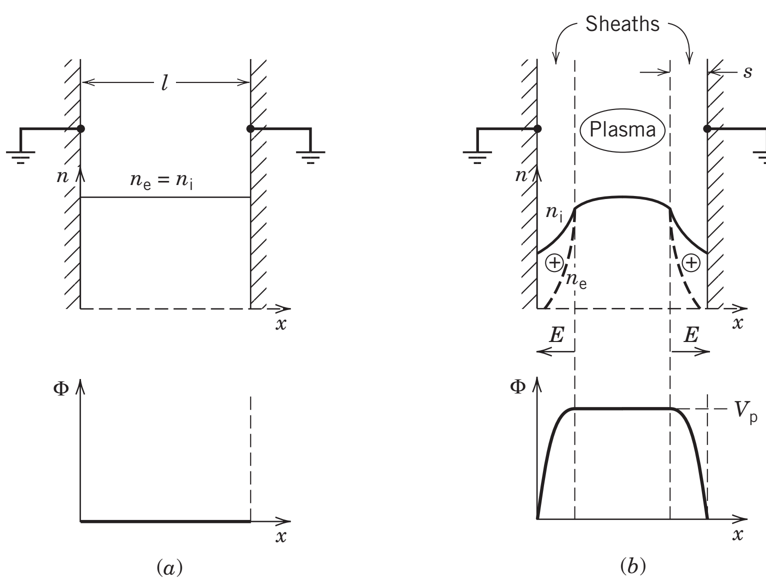

Figure 1.11 The formation of plasma sheaths: (a) initial ion and electron densities and potential; (b) densities, electric field, and potential after the formation of the sheath.

Figure 1.12 shows sheath formation as obtained from a particle-in-cell (PIC) plasma simulation. We use PIC results throughout this book to illustrate various discharge phenomena. In this simulation, the left wall is grounded, the right wall is floating (zero net current), and the positive ion density is uniform and constant in time. The electrons are modeled as $\mathcal{N}$ sheets having charge-to-mass ratio $-e/m$ that move in one dimension (along x) under the action of the time-varying fields produced by all the other sheets, the fixed ion charge density, and the charges on the walls. Electrons do not collide with other electrons, ions, or neutrals in this simulation. Four thousand sheets were used with $\mathrm{T_e} = 1$ V and $n_\mathrm{i} = n_\mathrm{e} = 10^{13}$ m^{-3} at time $t = 0$. In (a), (b), (c), and (d), we see the v_x–x electron phase space, electron density, electric field, and potential after the sheath has formed, at $t = 0.77$ μs. The time history of $\mathcal{N}$ is shown in (e); 40 sheets have been lost to form the sheaths. Figure 1.12a–d shows the absence of electrons near each wall over a sheath width $s \approx 6$ mm. Except for fluctuations due to the finite $\mathcal{N}$, the field in the bulk plasma is near zero, and the fields in the sheaths are large and point from the plasma to the walls. (E_x is negative at the left wall and positive at the right wall to repel plasma electrons.) The potential in the center of the discharge is $V_\mathrm{p} \approx 2.5$ V and falls to zero at the left wall (this wall is grounded by definition). The potential at the right wall is also low, but we see in (f) that it oscillates in time. We will see in Chapter 4 that these are *plasma oscillations*. We would not see them if the initial sheet positions and velocities were chosen exactly symmetrically about the midplane, or if many more sheets were used in the simulation.

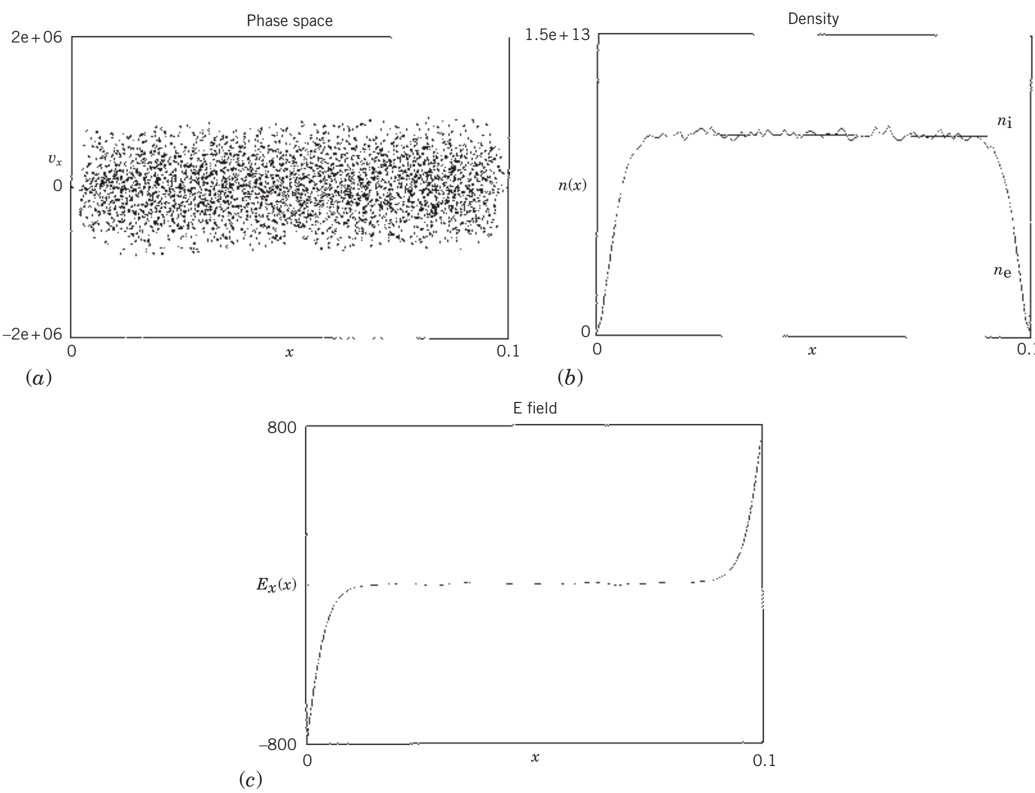

Figure 1.12 PIC simulation of positive ion sheath formation: (a) v_x–x electron phase space, with horizontal scale in meters; (b) electron density n_e; (c) electric field E_x; (d) potential Φ; (e) electron number $\mathcal{N}$ versus time t in seconds; (f) right hand potential v_x versus time t.

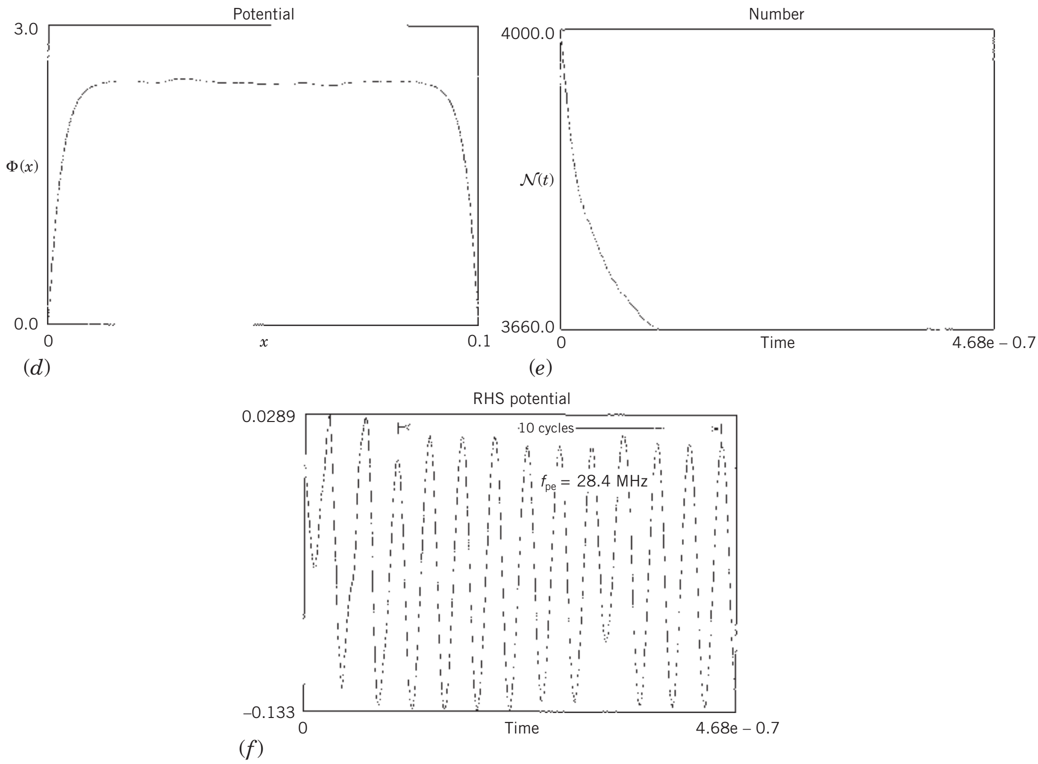

Figure 1.12 (*Continued*)

If the ions were also modeled as moving sheets, then on a longer timescale, we would see ion acceleration within the sheaths, and a consequent drop in ion density near the walls, as sketched in Figure 1.11*b*. We return to this in Chapter 6.

The separation of discharges into bulk plasma and sheath regions is an important paradigm that applies to all discharges. The bulk region is quasineutral, and both instantaneous and time-averaged fields are low. The bulk plasma dynamics are described by diffusive ion loss at high pressures and by free-fall ion loss at low pressures. In the positive space charge sheaths, high fields exist, leading to dynamics that are described by various ion space charge sheath laws, including low-voltage sheaths and various high-voltage sheath models, such as collisionless and collisional Child laws and their modifications. The plasma and sheath dynamics must be joined at their interface. As will be seen in Chapter 6, the usual joining condition is to require that the mean ion velocity at the plasma–sheath edge be equal to the ion-sound (Bohm) velocity: $u_B = (e\mathrm{T}_e/M)^{1/2}$, where e and M are the charge and mass of the ion and T_e is the electron temperature in volts.

1.3 Discharges

1.3.1 RF Diodes

Planar capacitively driven radio frequency (rf) discharges—so-called *rf diodes*—are a mainstay for materials processing. Early planar systems, as shown in Figure 1.13, were typically multi-wafer and used for anisotropic etches. This idealized discharge consists of a vacuum chamber containing two

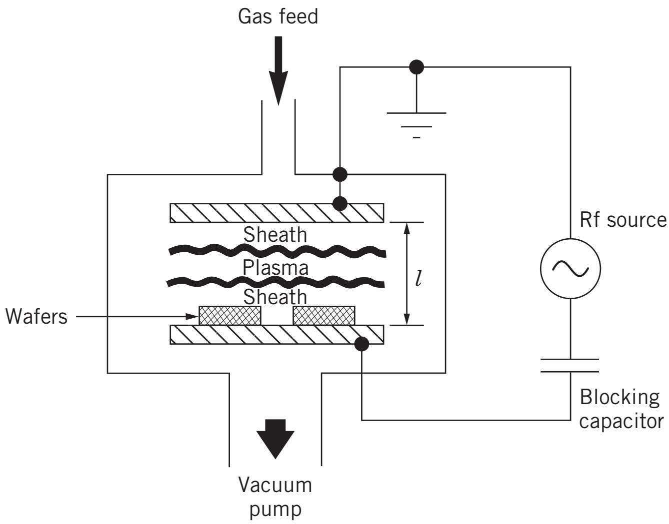

Figure 1.13 Typical multi-wafer capacitive rf discharge in plane-parallel geometry, used for anisotropic etching. Source: Lieberman and Gottscho (1994)/with permission of Elsevier.

Table 1.1 Typical Range of Parameters for RF Diode and High-Density Discharges.

Parameter	RF Diode	High-Density Source
Pressure p (mTorr)	3–3000	0.5–50
Power P (kW)	0.5–20	0.5–5
Frequency f (MHz)	0.05–60	2–2450
Cross-sectional area A (m^2)	0.1–10	0.1–1
Magnetic field B (kG)	0	0–1
Plasma density n (cm^{-3})	10^9–10^{11}	10^{10}–10^{12}
Electron temperature T_e (V)	1–5	2–7
Ion acceleration energy $\mathcal{E}_i$ (V)	200–1000	20–1000
Fractional ionization x_{iz}	10^{-6}–10^{-3}	10^{-4}–10^{-1}

Source: M. A. Lieberman, 2Ed modified

planar electrodes separated by a gap width l and driven by an rf power source. The substrates are placed on one electrode, feedstock gases are admitted to flow through the discharge, and effluent gases are removed by the vacuum pump. Typical parameters are shown in Table 1.1. The typical rf driving voltage is V_{rf} = 100–1000 V, and the plate separation is l = 2–10 cm. When operated at low pressure, with the wafer mounted on the powered electrode, and used to remove substrate material, such reactors are sometimes called reactive ion etchers (RIEs)—a misnomer, since the etching is a chemical process enhanced by energetic ion bombardment of the substrate, rather than a removal process due to reactive ions alone.

For anisotropic etching, typically pressures are in the range of 3–100 mTorr, powers per unit area are 3–30 kW/m^2, and driving frequencies are 13.56–60 MHz. Typical plasma densities are relatively low, 10^9–10^{11} cm^{-3}, and the electron temperature is of order 3 V. Ion acceleration energies (sheath voltages) are high, greater than 200 V, and fractional ionization is low. The degree of dissociation of the molecules into reactive species can range widely from less than 0.1% to nearly 100% depending on gas composition and plasma conditions. For deposition and isotropic etch applications, pressures tend to be higher, ion bombarding energies are lower, and frequencies can be lower than the commonly used standard of 13.56 MHz. The very large cross-sectional areas and powers shown for rf diodes in Table 1.1 are for processing large-area glass substrates for solar panels and flat panel displays.

The operation of capacitively driven discharges is reasonably well understood. As shown in Figure 1.14 for a symmetrically driven discharge, the mobile plasma electrons, responding to the instantaneous electric fields produced by the rf driving voltage, oscillate back and forth within the positive space charge cloud of the ions. The massive ions respond only to the time-averaged electric fields. Oscillation of the electron cloud creates sheath regions near each electrode that contains net positive charge when averaged over an oscillation period; i.e., the positive charge exceeds the negative charge in the system, with the excess appearing within the sheaths. This excess produces a strong time-averaged electric field within each sheath directed from the plasma to the electrode. Ions flowing out of the bulk plasma near the center of the discharge can be accelerated by the sheath fields to high energies as they flow to the substrate, leading to energetic-ion-enhanced processes. Typical ion-bombarding energies $\mathcal{E}_i$ can be as high as $V_{rf}/2$ for symmetric systems

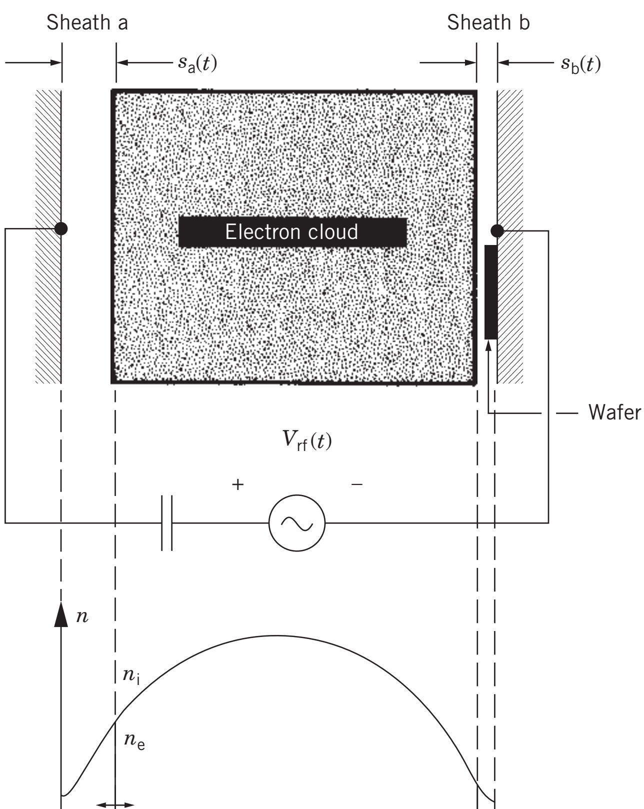

Figure 1.14 The physical model of an rf diode. Source: Lieberman and Gottscho (1994)/with permission of Elsevier.

(Figure 1.14) and as high as V_{rf} at the powered electrode for asymmetric systems, which have a powered electrode area greater than the area of the grounded electrode. A quantitative description of capacitive discharges is given in Chapter 11.

We note that the positive ions continuously bombard the electrode over an rf cycle. In contrast, electrons are lost to the electrode only when the oscillating cloud closely approaches the electrode. During that time, the instantaneous sheath potential collapses to near zero, allowing sufficient electrons to escape to balance the ion charge delivered to the electrode. Except for such brief moments, the instantaneous potential of the discharge must always be positive with respect to any large electrode and wall surface; otherwise, the mobile electrons would quickly leak out. Electron confinement is ensured by the presence of positive space charge sheaths near all surfaces.

We will see that a crucial limiting feature of rf diodes is that the ion-bombarding flux $\Gamma_i = nu_B$ and bombarding energy $\mathcal{E}_i$ cannot be varied independently. The situation is analogous to the lack of independent voltage and current control in diode vacuum tubes or semiconductor pn junctions. For a reasonable (but relatively low) ion flux, as well as a reasonable dissociation of the feedstock gas, sheath voltages at the driven electrode are high. For wafers placed on the driven electrode, this can result in undesirable damage, or loss of linewidth control. Furthermore, the combination of low ion flux and high ion energy leads to a relatively narrow process window for many applications. The low process rates resulting from the limited ion flux in rf diodes often mandate multi-wafer or batch processing, with consequent loss of wafer-to-wafer reproducibility. Higher ion and neutral fluxes are sometimes required for single-wafer processing in a clustered tool environment, in which a single wafer is moved by a robot through a series of process chambers. Clustered tools are used to control interface quality and offer significant cost savings in fabricating ICs. Finally, low fractional ionization poses a significant problem for processes where the feedstock costs and disposal of effluents are issues.

As shown in Figure 1.15*a*, modern capacitive discharges used for processing are almost always single-wafer systems. Furthermore, to meet the linewidth, selectivity, and damage control demands for critical etching and deposition steps, the mean ion bombarding energy, and perhaps its energy distribution, must be controllable independently of the ion and neutral fluxes. Some control over ion bombarding energy can be achieved by putting the wafer on the undriven electrode and independently biasing this electrode with respect to the chamber walls with a second rf source. However, processing rates are still low at low pressures and sputtering contamination is an issue. A more successful approach, shown in Figure 1.15*b*, is *dual frequency* operation, in which a high- and a low-frequency rf source are used to drive one or both plates of an rf diode. For well-separated frequencies, the high frequency mainly controls the ion flux and the low frequency controls the ion bombarding energy. Using a frequency higher than the conventional frequency of 13.56 MHz for the high-frequency drive results in an increased ion flux to the substrate for a fixed power input and allows the low-frequency drive to better control the ion energy. High frequencies of 27.12, 60, or 160 MHz, and low frequencies of 2 or 13.56 MHz, are used commercially.

Various magnetically enhanced rf diodes and triodes have also been developed to improve the performance of capacitive rf reactors. These include, for example, magnetically enhanced reactive ion etchers (MERIEs), shown in Figure 1.15*c*, in which a controllable dc magnetic field of 50–300 G is applied parallel to the powered electrode, on which the wafer sits. The magnetic field increases the efficiency of power transfer from the source to the plasma and also enhances plasma confinement. This results in a reduced sheath voltage and an increased plasma density when the magnetic field is applied. However, the plasma generated can be significantly nonuniform both radially and azimuthally. To increase process uniformity (at least azimuthally), the magnetic field is slowly rotated in the plane of the wafer, e.g., at a frequency of 0.5 Hz.

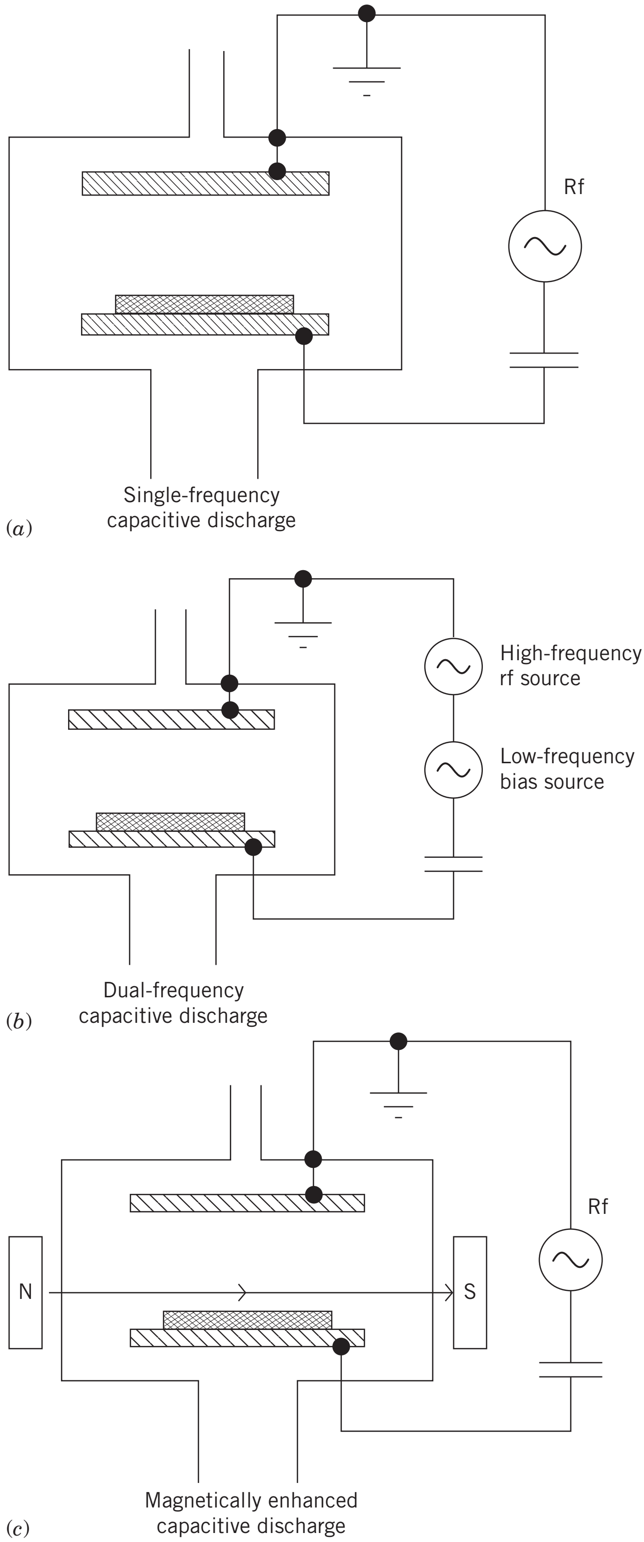

Figure 1.15 Some modern capacitive discharges are used for etching and deposition; (*a*) single frequency, (*b*) dual frequency, and (*c*) magnetically enhanced.

Low-pressure capacitive discharges are described quantitatively in Chapter 11. At higher pressures, typically ~ 0.2–10 Torr, the basic single-frequency capacitive configuration in Figure 1.15*a* is commonly used for PECVD. Important physical and chemical phenomena appear in this pressure range, including spatially varying electron temperatures and secondary electron emission from surfaces. At the higher pressures, the secondary emission can cause a transition to a new mode of operation in which the secondary electrons alone sustain the discharge, the so-called α–γ transition. Capacitive discharges can also be operated at atmospheric pressures with very narrow gap lengths, $l \sim 0.2$–3 mm, in a diffuse mode with relatively uniform transverse density profiles. We examine this high-pressure capacitive discharge regime quantitatively in Chapter 15.

1.3.2 High-Density Sources

The limitations of rf diodes and their magnetically enhanced variants have led to the development of new kinds of low-pressure, high-density plasma sources. In addition to dual-frequency capacitive discharges, three examples of non-capacitive discharges are shown schematically in Figure 1.16, and typical source and plasma parameters are given in Table 1.1. In addition to high density and low pressure, a common feature is that the rf or microwave power is coupled to the plasma across a dielectric window, rather than by direct connection to an electrode in the plasma, as for an rf diode. This noncapacitive power transfer is the key to achieving low voltages across all plasma sheaths at electrode and wall surfaces. Dc voltages, and, hence, ion acceleration energies, are then

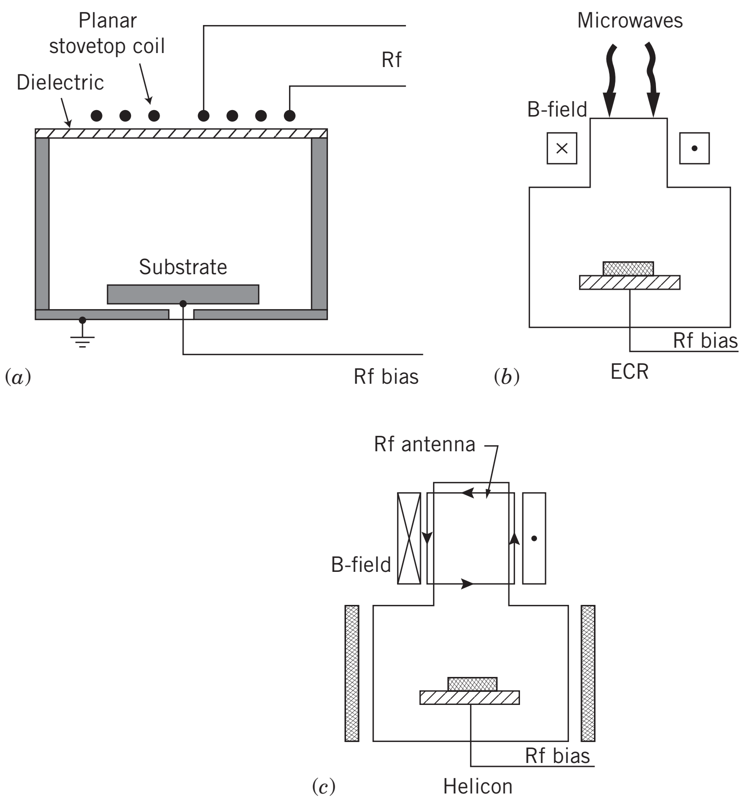

Figure 1.16 Some non-capacitive, high-density discharges used for etching and deposition; (*a*) planar inductive; (*b*) electron cyclotron resonance; (*c*) helicon.

typically 20–30 V at all surfaces. To control the ion energy, the electrode on which the wafer is placed is independently driven by a capacitively coupled rf source. Hence, independent control of the ion/radical fluxes (through the source power) and the ion-bombarding energy (through the wafer electrode power) is possible.

The common features of power transfer across dielectric windows and separate bias supply at the wafer electrode are illustrated in Figure 1.16. However, sources differ significantly in the means by which power is coupled to the plasma. A planar inductive (or transformer) coupled source is shown in Figure 1.16*a*. Here, the plasma acts as a single-turn, lossy conductor that is coupled to a multi-turn nonresonant rf coil across the dielectric discharge chamber; rf power is inductively coupled to the plasma by transformer action. We describe inductive discharges quantitatively in Chapter 12.

For the electron cyclotron resonance (ECR) source shown in Figure 1.16*b*, one or more electromagnet coils surrounding the cylindrical source chamber generate an axially varying dc magnetic field. Microwave power is injected axially through a dielectric window into the source plasma, where it excites a right-hand circularly polarized wave that propagates to a resonance zone, for cold electrons at $\omega = \omega_{ce}$, where the wave is absorbed. Here, $\omega = 2\pi f$ is the applied radian frequency and $\omega_{ce} = eB/m$ is the electron gyration frequency at resonance. For the typical microwave frequency used, $f = 2450$ MHz, the resonant magnetic field is $B \approx 875$ G. The plasma streams into the process chamber in which the wafer is located.

A helicon source is shown in Figure 1.16*c*. A weak (50–200 G) dc axial magnetic field together with an rf-driven antenna placed around the dielectric cylinder that forms the source chamber allows excitation of a helicon wave within the source plasma. Resonant wave–particle interaction is believed to transfer the wave energy to the plasma. ECR and helicon sources are described quantitatively in Chapter 13.

Figure 1.16 also illustrates the use of high-density sources to feed plasma into a relatively distinct, separate process chamber in which the wafer is located. As shown in Figure 1.16*c*, the process chamber can be surrounded by dc multipole magnetic fields to enhance plasma confinement near the process chamber surfaces, while providing a magnetic near-field-free plasma environment at the wafer. Such configurations are often called “remote” sources, a misnomer since at low pressures considerable plasma and free radical production occurs within the process chamber near the wafer. Sometimes, the source and process chambers are more integral, e.g., the wafer is placed very near to the source exit, to obtain increased ion and radical fluxes, reduced spread in ion energy, and improved process uniformity. But the wafer is then exposed to higher levels of damaging radiation.

Although the need for low pressures, high fluxes, and controllable ion energies has motivated high-density source development, there are many issues that need to be resolved. A critical issue is achieving the required process uniformity over 300-mm wafer diameters. In contrast to the nearly one-dimensional geometry of typical rf diodes (two closely spaced parallel electrodes), high-density cylindrical sources can have length-to-diameter ratios of order or exceeding unity. Plasma formation and transport in such geometries are inherently radially nonuniform. Another critical issue is efficient power transfer (coupling) across dielectric windows over a wide operating range of plasma parameters. Degradation of and deposition on the window can also lead to irreproducible source behavior and the need for frequent, costly cleaning cycles. Low-pressure operation leads to severe pumping requirements for high deposition or etching rates and, hence, to the need for large, expensive vacuum pumps. Furthermore, plasma and radical concentrations become strongly sensitive to reactor surface conditions, leading to problems of reactor aging and process irreproducibility. Finally, dc magnetic fields are required for some source concepts. These can lead to magnetic field-induced process nonuniformities and damage.

In addition to rf and microwave discharges, magnetically enhanced dc discharges are widely used for sputtering metal and dielectric films from a cathode “target” onto a substrate placed on the anode electrode. Sputtering of target atoms onto the substrate is induced by ions that flow across the 500–1000 V cathode sheath. Figure 1.17 illustrates a dc planar magnetron discharge, which is widely used for such depositions and also has important applications for the coating of large rectangular sheets of architectural glass. Such discharges can also be driven by rf and pulsed voltages. Various other types of dc discharges are also used. We examine dc discharges, quantitatively, in Chapter 14.

Figure 1.18 illustrates schematically the central problem of discharge analysis, using the example of an rf diode. Given the *control* parameters for the power source (frequency ω, driving voltage V_{rf}, or absorbed power P_{abs}), the feedstock gas (pressure p, flow rate, and chemical composition), and the geometry (simplified here to the discharge length l), then find the *plasma* parameters, including the plasma density n_i, the etchant density n_F, the ion and etchant fluxes Γ_i and Γ_F hitting the substrate, the electron and ion temperatures T_e and T_i, the ion bombarding energy $\mathcal{E}_i$, and the sheath thickness s. The control parameters are the "knobs" that can be "turned" in order to "tune" the properties of the discharge.

The tuning range for a given discharge is generally limited. Sometimes one type of discharge will not do the job no matter how it is tuned, so another type must be selected. As suggested in Figures 1.15–1.17, a bewildering variety of discharges are used for processing. Some are driven by rf, some by dc, and some by microwave power sources. Some use magnetic fields to increase the plasma confinement or the efficiency of power absorption. One purpose of this book is to guide the reader toward making wise choices when designing discharges used for processing.

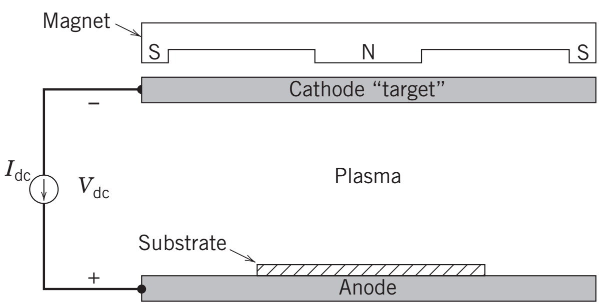

Figure 1.17 A dc planar magnetron discharge, used for thin film deposition.

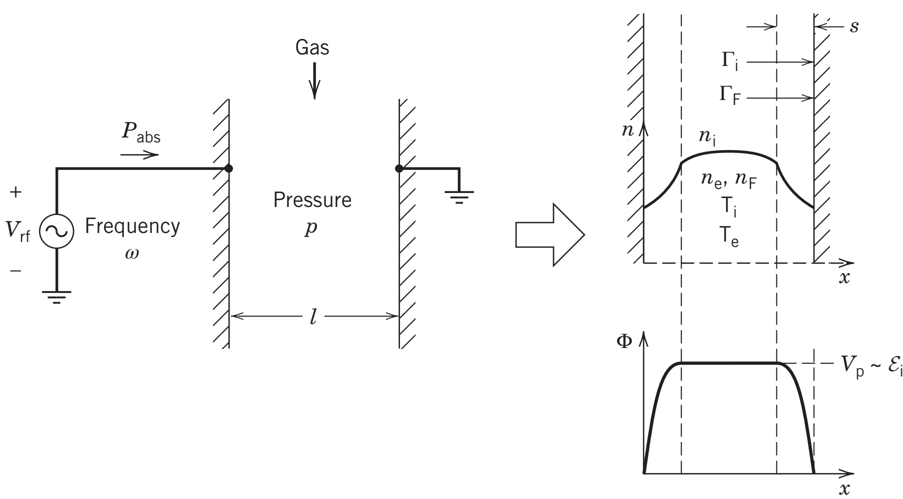

Figure 1.18 The central problem of discharge analysis.

1.4 Symbols and Units

The choice of symbols is always vexing. While various fields each have their consistent set of symbols to represent physical quantities, these overlap between different fields, e.g., plasma physics and gas-phase chemistry. For example, H is not only standard for enthalpy in chemistry but also standard for magnetic field in plasma physics. This also occurs within a given field, e.g., k is standard not only for Boltzmann's constant but also for wave number. Then, there is always the occasional symbol that must stand for many things in different contexts. We sometimes distinguish these by using different lettering (Roman, italic, script, and boldface), e.g., I is a current and I is a modified Bessel function; M is an ion mass and $\mathcal{M}$ is the number of chemical species. We can often distinguish commonly used symbols by the use of subscripts, e.g., σ denotes a cross section, but σ_{rf} and σ_{dc} denote electrical conductivities; we have done this whenever the notation is not too cumbersome. The meaning should be clear from the context, in most cases. To help avoid confusion, we have provided a table of symbols and abbreviations in the front matter of this book. These give the normal usage of symbols and their units.

As far as possible, we use the SI (MKS) system of units: meters (m), kilograms (kg), seconds (s), and coulombs (C) for charge. In these units, the charge on an electron is $-e \approx -1.602 \times 10^{-19}$ C. The unit of energy is the joule (J), but we often use the symbol $\mathcal{E}$ for the voltage that is the equivalent of the energy, i.e.,

$$U(\text{joules}) = e\mathcal{E}$$

where $\mathcal{E}$ is in volts. We also occasionally use the calorie (cal): 1 cal $\approx$ 4.187 J. The SI unit of pressure is the pascal (Pa), but we more commonly give gas pressures in Torr:

$$1\,\text{Torr} \approx 133.3\,\text{Pa}$$

We occasionally use 1 atm $\approx 1.013 \times 10^5$ Pa $\approx$ 760 Torr and 1 bar $= 10^5$ Pa to refer to gas pressures. The SI unit for the magnetic induction B is tesla (T), but we often give B in gauss (G): 1 T $= 10^4$ G. We use the italic typeface symbol T to refer to the temperature in kelvins (K). The energy equivalent temperature in joules is kT, where $k \approx 1.381 \times 10^{-23}$ J/K is Boltzmann's constant. We often use the roman typeface symbol T for the voltage equivalent of the temperature, where

$$e\mathrm{T}(\text{volts}) = kT(\text{kelvins})$$

Hence, room temperature $T = 297$ K is equivalent to $\mathrm{T} \approx 0.026$ V. Even within the standard unit system, quantities are often designated by subunits. For example, cross sections are often given in cm^2 rather than m^2 in tables, and wavelengths at microwave frequencies are commonly given in cm rather than in meters.

To assist our readers in making calculations, we give the commonly used constants in the SI system of units and the most common conversions between units in the front matter of the book. It is sometimes tempting to make a calculation in nonstandard units. For example, the collision frequency $\nu = n\sigma v$, which has units $(\text{m}^{-3} \cdot \text{m}^2 \cdot \text{m}\,\text{s}^{-1})$, could equally well be calculated in the commonly used units $(\text{cm}^{-3} \cdot \text{cm}^2 \cdot \text{cm}\,\text{s}^{-1})$, since the length units cancel. However, we urge the student not to take such shortcuts, but to systematically convert to standard units, before making a calculation.